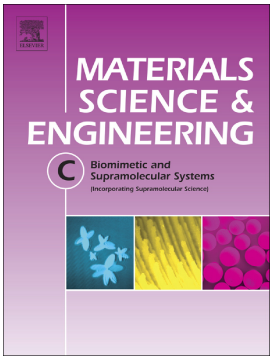

Core-clad phosphate glass fibers for biosensing

A. Mishra, F. Désévédavy, L. Petit, F. Smektala, J. Massera

PII: S0928-4931(18)30161-9
DOI: https://doi.org/10.1016/j.msec.2018.11.038
Reference: MSC 9058

To appear in: *Materials Science & Engineering C*

Received date: 16 January 2018
Revised date: 14 November 2018
Accepted date: 24 November 2018

Please cite this article as: A. Mishra, F. Désévédavy, L. Petit, F. Smektala, J. Massera , Core-clad phosphate glass fibers for biosensing. Msc (2018), https://doi.org/10.1016/j.msec.2018.11.038

Core-clad phosphate glass fibers for biosensing

A. Mishra[1], F. Désévédavy[2], L. Petit[3], F. Smektala[2], J. Massera[1]

[1] *Faculty of Medicine and Health Technology, Tampere University, Korkeakoulunkatu 10, FI-33720 Tampere, Finland*

[2] *Laboratoire Interdisciplinaire Carnot de Bourgogne, UMR 6303 CNRS-Université de Bourgogne Franche-Comté, 9 Av. A. Savary, 21078 Dijon, France*

[3] *Laboratory of Photonics, Tampere University, Korkeakoulunkatu 10, FI-33720 Tampere, Finland*

Abstract

Recently, a phosphate glass with composition 20 CaO - 20 SrO - 10 Na_2O - 50 P_2O_5 (mol%) was found to have good potential as a biomaterial and to possess thermal properties suitable for fiber drawing. This study opened the path towards the development of fully bioresorbable fibers promising for biosensing. In the past, this phosphate glass with CeO_2 was found to increase the refractive index and the glass stability. Therefore, a new SrO-containing glass was prepared with 1 mol% of CeO_2 and core fibers were drawn from it. A core-clad fiber was also processed, where the core was a Ce-doped glass and the clad undoped, to allow for total internal reflection. The mechanical properties of the core and core-clad fibers are discussed as a function of immersion time in TRIS-buffer solution. Finally, a sensing region was created, in the core-clad fiber, by etching the cladding using phosphoric acid. Then, the change in light transmission, upon immersion in TRIS-buffer solution, was quantified to assess the potential use of the novel core-

clad fiber as a biosensor. Upon immersion in TRIS, the core-clad fiber was found to guide light effectively and to maintain a tensile strength of ~ 150-200 MPa up to 6 weeks in TRIS, clearly showing that this fiber has potential as a biosensing device.

Introduction

Phosphate glasses (PGs) have emerged as good alternatives to the traditional silicate glasses for biomedical applications. Silicate glasses have long been the popular choice as bioactive glasses among researchers, since the discovery of 45S5 by Hench *et al.* [1]. However, the processability of silicate glasses into scaffold, fibers etc. is hindered due to their crystallization kinetics [2-3]. Meanwhile, phosphate glasses have emerged as promising candidates as bioactive materials due to their unique properties: they are completely biodegradable, and their composition can be adjusted to attain desirable degradation rates (from weeks to years) [4]. Moreover, phosphate glasses possess excellent thermal properties enabling fiber drawing without adverse crystallization [4-7]. A detailed study of the potential use and benefits of PGs, in the medical field, can be found in [8].

Glass fibers have been researched extensively both in the medical and optical research fields. Degradable bioactive glass fibers can be used in composites to improve the mechanical properties of scaffolds and of other biomedical devices [9]. Similar to the bulk glasses, phosphate glass fibers have been found to be particularly suitable not only for bone repair and reconstruction but also in soft tissue engineering applications [10-14]. From an optics perspective, the potential of ~~using~~ glass fibers as biosensors has been investigated in detail in [15]. Their potential in tracking glass dissolution is discussed in [16]. Additionally, phosphate fibers exhibit high transparency in the UV-Visible/Near infrared (UV-Vis/NIR) range, and their

refractive index is comparable to the commercially available silicate glass fibers [17-19].

Glass with composition $50P_2O_5$-20SrO-20CaO-$10Na_2O$ (mol%), referred to as Sr50 has favorable degradation characteristics for potential use in biomedical applications as reported in [20]. When Sr50 is doped with CeO_2 (from 1 to 7 mol%), the glass network becomes more cross-linked and therefore more resistant to dissolution delaying the precipitation of a reactive surface layer a~~t the surface of the glass~~ [7]. The CeO_2 doping was done such that the (Ca+Sr)/P remained the same than in Sr50, thereby not affecting its ability to form a Ca-Sr-P layer at the surface. The resistance to crystallization, of these CeO_2 doped glasses, increased compared to the Sr50 [7]. Furthermore, the addition of CeO_2 leads to an increase in the refractive index, allowing the drawing of core-clad fiber from Sr50 (Clad) and a Ce-doped-Sr50 composition (core) having suitable Δn (where $\Delta n = n_{core} - n_{clad}$ is positive) for total internal reflection. In this study, core and core-clad preforms were drawn into fibers to determine their suitability for biosensing. Core fibers were drawn from the Sr50 glass and Ce-1 glass with the [0.99 ($50P_2O_5$-20SrO-20CaO-$10Na_2O$) – $1CeO_2$ (mol%)] composition, with a diameter of (140±10) µm and (110±10) µm respectively. For the core-clad fiber, Ce-1 glass was chosen as the core, and Sr50 as the cladding, and fibers were drawn with a diameter of (140±10) µm from preform produced using a homemade rotational caster.

In this paper, we investigated the effect of in-vitro dissolution of the fibers on their mechanical and optical properties. In the core-clad fibers, a sensing region was produced by selectively etching the cladding, revealing the core of the fiber. Then, light loss of the etched core-clad fibers was measured as a function of immersion time in TRIS. The mechanical properties of the etched core-clad fibers, were also ascertained. Additionally, the impact of immersion in TRIS buffer on the mechanical properties of the fibers was obtained.

Materials and Methods

1) **Preform preparation and fiber drawing** –

Core preforms: The core preforms with the composition [$50P_2O_5$-20SrO-20CaO-$10Na_2O$] (labeled as Sr50) and [0.99 ($50P_2O_5$-20SrO-20CaO-$10Na_2O$) – $1CeO_2$ (mol%)] (labeled as Ce-1) were prepared by melting batches of 45g comprising of $Ca(PO_3)_2$, $Sr(PO_3)_2$, $NaPO_3$ (and CeO_2 for Ce-1 composition) at 1100 °C (heating rate 10 ^oC/min) for 30 min. $Ca(PO_3)_2$ and $Sr(PO_3)_2$ were prepared beforehand by heating $NH_4H_2PO_4$ with $CaCO_3$ and $SrCO_3$ respectively, in separate batches. The batch was heated to 250 °C for 12 h, then to 650 °C for 12 h and finally to 850 °C for 12 h at 1 °C.min^{-1} to remove CO_2, NH_3 and H_2O. After melting, the molten batch was cast into a 10 cm long pre-heated (350 ^oC) brass mold having a diameter of 12 mm, and annealed at 15 °C below their respective glass transition temperature for 15 h, to obtain a mechanically stable preform. Annealing was performed below T_g to decrease the risk of nuclei formation.

Core-clad preform: The core-clad preform, with core Ce-1 and clad Sr50, was prepared using a homemade rotational caster. The clad composition was first poured in a pre-heated brass mold (350 ^oC), which is then spun at 1000 rpm for 10 sec. The spinning results in the formation of a hollow cylinder in the mold. Then the core composition is poured slowly inside the hollow cladding. The preform was then annealed similarly as for the core preforms. The process was optimized as in [21] to guarantee a constant $Ø_{clad}/ Ø_{core}$, before and after drawing. The small CeO_2 addition to the glass composition did not lead to a significant change in thermal expansion coefficient and all the processed core-clad preforms were free of cracks or any defects.

Fiber drawing: Fibers were drawn using the "rod" method in a specially designed single zone drawing tower furnace. To prevent nucleation or crystallization, the temperature profiles of this furnace were precisely mapped beforehand, and the dwell time in the zones was controlled prior to and during the drawing. Thermal profiles for different setting temperatures were performed by means of a thermocouple attached to the preform motion cane. After waiting for the furnace to stabilize to the set temperature, the thermocouple was gradually moved down into the furnace. In the meantime the thermocouple temperature and position were registered, as presented in Fig-1. The drawing temperature was 645 °C for all the fibers under an inert He gas laminar flow of 2.5 $L.min^{-1}$. This temperature corresponded to a set temperature of 770 °C (Fig-1). The high thermal conductivity K_{He} of helium allowed to minimize the dwell time before drop formation and during drawing, $K_{He} = 33{,}63.10^{-5}$ $cal.sec^{-1}.cm^{-1}.{}^{o}C^{-1}$, $K_{Ar} = 4{,}06.10^{-5}$ $cal.sec^{-1}.cm^{-1}.{}^{o}C^{-1}$, $K_{air} = 5.68.10^{-5}$ $cal.sec^{-1}.cm^{-1}.{}^{o}C^{-1}$ [22]. The drawing temperature was determined based on the glass transition temperature (T_g) and the furnace thermal profile. The glass rod was placed into the furnace and the temperature gradually increased above T_g until the formation of a drop. During the drawing, the temperature was adjusted based on readings from the tension measurement gauge. The fiber was then fixed on a rotary drum, while the fiber diameter and drawing tension were controlled by a computer system based on LabView software.

2) **Optical properties** – A fully automated Metricon, model 2010 prism coupled refractometer was used to measure the refractive index of 2 mm thick glass samples of bulk core and cladding glass samples at 1060 nm. The accuracy of the measurement was ±0.0001. The samples were polished with SiC polishing paper (600, 800, 1200, 2400 and 4000 grit) on both faces.

3) **Immersion tests** – Immersion tests were carried out by immersing the fibers in TRIS buffer solution for up to 6 wks. For each immersion time point, 10 fibers of length 15 cm were entirely

immersed in 50 ml of TRIS, and were placed in an incubating shaker HT Infors Multitron at 37 °C, 100 rpm to obtain laminar flow mixing without moving the fibers.

4) **Mechanical testing** – Mechanical tests were performed, in tension (static), on the core and core-clad fiber prior to and after immersion in TRIS. Post immersion, the core and core-clad fibers were carefully collected, rinsed with acetone and dried in air, overnight, in an incubator at 37 ºC. The specimens were then maintained in desiccator before testing. Mechanical strength measurements were carried out at ambient temperature using Instron 4411 Materials Testing Machine, with a grip distance of 50 mm, a load cell of 500 N, and a crosshead speed of 30 $mm.min^{-1}$. The grips were covered with a rubber mat to avoid slipping of the fiber during the test and damage caused by the metallic grips. The tensile strength and the Young's modulus were calculated as the mean of 10 test fibers. Despite the low number of ~~the~~ specimens, the Weibull modulus was estimated as reported in [23-24].

5) **Light loss** –

The fibers' optical losses were measured using the cut back technique. The signal from the FTIR spectrometer transmitted through a long piece of fiber (L_1) was recorded (I_1), using a nitrogen cooled InSb detector. Then, without moving the input end, the fiber was cut (cleaved) and the output fiber signal was recorded (I_2). From the measurement of the cut length corresponding to L_1-L_2, the signals I_1 and I_2, the losses were calculated by using the following equation:

$$\text{Losses (dB/m)} = \frac{10}{L_1 - L_2} \times \log\left(\frac{I_2}{I_1}\right).$$

The same measurement was repeated several times to increase accuracy.

The light transmission, as a function of immersion time, was measured in the wavelength range of 200-1000 nm. A 50 cm long fiber, was connected on one end to a light source and at the other end to a spectrometer. The fibers were cleaved and coupled using FC connector (Thorlabs). The lamp position was adjusted to maximize the light intensity at the fiber output. A 5 cm portion (sensing region) of the fiber was immersed in TRIS. For the illumination, a broadband white light source (Edmund BDS130) was used, and a ThorLabs Compact Spectrometer CCS200 was used for collecting the light. The light accumulation was set to 7.5 ms to maximize the signal. The light intensity recorded at 680 nm was tracked as a function of immersion time. The signal was normalized to 1 prior to immersion and only the relative intensity is reported. The TRIS solution was refreshed each week in order to avoid significant evaporation of the solution. Evaporation would increase the surface area to volume of the solution ratio, leading to a change in the dissolution rate.

6) **Microscopy –** The core-clad fibers were collected post mechanical tests for imaging. They were imaged along their length using optical microscope Olympus BH2-UMA to evidence the deposition of a surface layer after immersion in TRIS. The optical microscope was also used to measure the initial and post-immersion fiber diameter. The fibers cross-section, post fracture was also visualized using Zeiss ULTRAplus scanning electron microscope (SEM)

Results and discussion

To guide the light successfully, a core-clad fiber should be drawn using glasses with specific refractive index (n) to allow total internal reflection of the light: the n_{core} should be greater than n_{clad}. Here, the glasses under investigation were [$50P_2O_5$-20SrO-20CaO-$10Na_2O$] (labeled as

Sr50) and [0.99 ($50P_2O5$-20SrO-20CaO-$10Na_2O$) – $1CeO_2$ (mol%)] (labeled as Ce-1) with a refractive index at 1060nm of 1.5261 and 1.5345, respectively. Core fibers were drawn from Sr50 and Ce-1 glasses with a diameter of (~140±10) and (~110±10) µm, respectively.

A core-clad fiber was drawn using Sr50 glass as the clad and the Ce-1 as the core, ~~of the fiber~~ with a total diameter of (~140±10) µm. This fiber had a numerical aperture NA of 0.16, which is similar to the NA of some of our earlier studied fibers [21]. The preparation of fiber with such large NA guarantees the proper light guiding through the core of the fiber, as confirmed by the optical image of the core-clad fiber cross-section, presented in Fig-2. The step index difference between the core and the clad can be seen on the micrograph by the bright coloration of the core compared to that of the cladding [25]. The clad diameter was 140 µm as targeted, with a core diameter of 75 µm.

The attenuation spectra of the core fibers are shown in Fig-3. The optical losses of the Sr50 and Ce-1 core fibers were around 20 and 10 dB/m, respectively. The lower optical losses in the Ce-1 fiber compared to that of Sr50 fiber was attributed to an increase in the network cross-linking due to the doping with CeO_2. Indeed, most of the phosphate glasses used as laser are within the metaphosphate structure and contain large amount of Al_2O_3. The aim of Al^{3+} ions in the glass is to increase the connectivity between the phosphate chains that in turn reduce the light loss [26]. The core-clad fiber was found to have similar light losses than the Ce-1 core fiber at 1.55 µm.

The core fibers (Sr50 and Ce-1) and the core-clad fiber were immersed in TRIS buffer solution for up to 42 days. The change in the fibers' mechanical properties (namely tensile strength, Young's modulus and Weibull modulus) as a function of days in TRIS are reported in Figs-4. Prior to immersion (t=0), the Sr50 and Ce-1 core fibers exhibit similar tensile strength at ~550

MPa indicating that the preform processing and fiber drawing of these two glass compositions lead to similar density of surface defects (Fig-4a). However, the core-clad fibers exhibit lower tensile strength compared to the core fibers. This can be attributed to the manufacturing process; for example, coefficient of thermal expansion mismatch between the core and the clad could cause a drop in the mechanical properties [27-29]. This is in agreement with [30]: Ahmed et al. reported on the processing of core-clad fibers obtained via extrusion. In their study, a glass with composition $50P_2O_5$-16CaO-$5Na_2O$-24MgO-$5Fe_2O_3$ (P50Fe5) was extruded together with a glass with composition $45P_2O_5$-16CaO-$10Na_2O$-24MgO-$5TiO_2$ (P45Ti5) to obtain fiber with 39-45 µm diameter. These core-clad fibers ~~obtained~~ exhibited an average tensile strength of 302 ± 73 MPa and 236 ± 53 MPa when the glass P50Fe5 was used as clad (P45Ti5 as core) and core (P45Ti5 as clad) respectively. Sharmin et al. reported a tensile strength of ~526 ± 110 MPa for a fiber drawn from the P45Fe5 composition with diameter of ~20 µm [31]. This clearly indicated that the processing of core-clad fibers might negatively influence the mechanical properties of the fiber. The origin of the fibers' fracture was investigated using optical microscopy. The core and core-clad fibers were inspected and two examples of the cross-section of fibers are given in Figs-5: (a) presents the optical microscope image of the core fiber (Ce-1) and (b) the core-clad fiber cross-section while (c) presents the SEM micrographs of the core fiber and (d) the core-clad fibers cross section post-fracture. From Figs-5, one can see the surface fracture origin, the mirror and the hackles, as evidenced in [32]. Fig-5b does not show the hackles as clearly as in Fig-5a but can clearly be seen in Fig-5d. In all cases, even for the core-clad fibers, the surface fracture origin was located at the cladding surface. No core-clad fibers were found to break at the core-clad interface. Therefore, the low mechanical properties of the core-clad fiber seen in Fig-4, did not come from defects at the core-clad interface.

As seen in Fig-4a, upon immersion for 2 days, an increase in tensile strength of all the fibers was observed. Such ~~an~~ increase ~~in tensile strength~~, upon immersion, was also evidenced in [33] and was due to the etching of the fiber surface, which reduced the amount of surface defects. At longer immersion time, a decrease in tensile strength of the Sr50 fiber was measured due to the corrosion of the fiber [34]. However, the tensile strength of the Ce-1 fiber started to decrease only after 21 days in TRIS. The delay in the decrease of the Ce-1 fiber's mechanical properties may be attributed to the presence of Ce in the Sr50 glass network, which was found to drastically reduce the glass reactivity in aqueous solution (both dissolution and precipitation of a reactive layer) as explained in [8]. The core-clad fiber exhibited similar changes in the mechanical properties than the Sr50 core fiber. However, the increase in tensile strength of the core-clad fiber during the first two days of immersion was lower compared to the Sr50 core fiber. This might be related to a high density of large defects at the core-clad fiber surface, which cannot be efficiently etched. It should be pointed out that all the fibers exhibited a similar tensile strength of about 150 MPa after 42 days in TRIS.

Fig-4b presents the Young's modulus of the investigated fibers as a function of immersion time in TRIS. Initially (at t=0), the core-clad and the Sr50 core fibers exhibit similar Young's modulus. The Ce-1 core fiber exhibits a larger Young's modulus probably due to the ~~slight~~ increase in network connectivity when adding CeO_2 in the glass network [7]. While the fibers in [33, 35] were reported to maintain their Young's modulus, upon immersion in buffer solution, the investigated fibers exhibited a Young's modulus which increased initially and then decreased upon immersion in TRIS. Surprisingly, the Young's modulus of the fibers increased during the first few days in TRIS. The Young's modulus for Sr50 and the core-clad fibers exhibited a maximum after 7 days in TRIS while that of the Ce-1 fiber exhibited a maximum during 21 days

in TRIS due to its slower reactivity. A similar increase in the tensile modulus post-annealing of the fibers was reported in [33] and ~~the increase in the modulus~~ was assigned to structural changes. It is also accepted that the mechanical properties of phosphate glasses are a function of compositional parameters (dissociation energy and packing density) and the total bonding energy [36-37]. Despite the dissolution of these glasses being considered as congruent, the surface of the fiber is expected to undergo alkaline and alkaline earth depletion as reported in [38]. The change in the fiber surface composition can lead to an initial increase in the Young's modulus. The drop in the modulus was then related to pitting and local defect formation upon selective dissolution of areas with higher reactivity.

Immersion of fibers is also known to affect the probability of early fracture and therefore the scatter in brittle fracture strength, as defined by the Weibull modulus [39]. Weibull modulus of the fibers as a function of immersion time is presented in Fig-4c. A high modulus indicates low scatter in brittle fracture strength and, thus, a higher strength reproducibility. Both the core-clad and the Ce-1 fibers exhibited an initial rise in the Weibull modulus which then drops at longer immersion times in TRIS. The initial increase in the Weibull modulus was expected, as the etching of the fiber is expected to remove the largest surface flaws decreasing then the probability of a fiber to undergo premature breakage. This, in turn, reduces the scatter in brittle fracture strength. The decrease in the Weibull modulus of fibers immersed for longer immersion time indicated that ~~at long immersion in TRIS,~~ the surface flaws started to increase, leading to fibers with early fracture (lower tensile stress) and higher scatter in brittle fracture.

In the past, it was demonstrated that the changes in the optical properties of a core bioresorbable bioactive glass fibers, upon immersion in SBF, could give information regarding the state of degradation [16]. To reveal a sensing region, the clad of the core-clad fiber was etched away.

Etching was performed using 1M phosphoric acid. Fig-6 exhibits the reduction in diameter of the core-clad fiber as a function of etching time ~~in phosphoric acid~~. The fiber diameter decreased almost linearly at a rate of 4.4 $\mu m.h^{-1}$. Therefore, the clad was suspected to be completely etched away after 14.5 h ~~of etching~~. Fig-7 presents the optical images of the cross-section of the partially etched fiber after 13h of immersion in 1M H_3PO_4, showing near complete removal of the clad.

Etching of the fiber was suspected to have an effect on the fiber's mechanical properties as reported in [40]. Fig-8a, depicts the tensile strength of 10 etched core-clad fibers (etching time was 14.5 h to fully remove the cladding). The fibers were not all fractured in the etched region. Fig-8b presents a schematic of the location of the fracture origin. Out of the 10 fibers, four broke at the interface between the etched and un-etched region (Region I), four broke in the etched region (Region II) and two broke in the un-etched part (Region III). The average tensile strength was ~225 MPa, ~150 MPa and ~350 MPa, in Region I, II and III, respectively (Fig. 8a). This clearly shows that the etching of the fibers led to a decrease in the fiber mechanical properties due to an increase in flaw density, formation of surface pits, a decrease in the fiber diameter and/or an increase in the size of surface flaws. Indeed, mild etching, obtained using dissolution of the fiber in TRIS initially increased the mechanical properties (such as tensile or bending strength), while at longer dissolution time the mechanical properties decreased most likely due to an increase in the fiber roughness and/or due to the precipitation of a reactive calcium phosphate layer at the fibers' surface [40]. It is also interesting to point out that the low tensile strength of the etched fibers are similar to that of fibers immersed for extended period of time in TRIS. This supported our hypothesis that upon significant surface etching, ~~it is~~ the increase in ~~the~~ surface roughness and ~~in the~~ surface flaws ~~which~~ dictate the fiber's failure.

The sensing region (5 cm) was immersed in TRIS buffer solution for up to 42 days. Fig-9 shows the light loss through the etched portion of a core-clad fiber. A progressive reduction in the relative intensity of the output light at 680 nm of the core-clad fiber can be observed upon immersion in TRIS. Fig-10 presents the optical micrographs of the etched fiber upon immersion for a) 7 days, b) 21 days and c) 42 days as well as the SEM image of the fiber surface upon immersion for 42 days. The rapid decrease in light intensity, during the first 14 days, was attributed to the fast initial dissolution of the glass in aqueous solutions and a decrease in the fiber diameter. At longer immersion time, it is clear from Figs-10 (b, c and d) that a thin CaP reactive layer precipitated at the surface of the fiber ~~as seen in [16]~~, the thickness of which grew overtime leading to further increase in the light losses as discussed in [16]. When compared to our former study in [7], the layer precipitated at a slower rate when immersed in TRIS than in SBF, as SBF solution is known to be thermodynamically unstable and to lead to rapid precipitation of a reactive layer [41]. It is interesting to point out that, from SEM analysis the reactive layer was fine and not well attached to the glass surface as already shown in [20] ~~which~~ confirming the role of the reactive layer formation on the decreased mechanical properties reported here.

Conclusions

Core (Sr50 and Ce-1) and core (Ce-1)-clad (Sr50) phosphate fibers were successfully drawn into fibers. The tensile strength of the core-clad fibers was lower compared to that of the core and was assigned to an increase in the density of the core-clad fiber surface defects ~~at the~~ surface of the fiber. Upon immersion in TRIS for 2 days, all the fibers exhibited an increase in mechanical

properties (tensile strength, Young's modulus and Weibull modulus) due to the etching of the fibers' surface and a subsequent decrease in the density of surface defects. At longer immersion, the mechanical properties of the fibers dropped due to the dissolution/reaction of the glass with the aqueous media. The drop in mechanical properties of the fibers was delayed by the presence of CeO_2. The change in the mechanical properties of the core-clad fibers followed a similar trend than the Sr50 core fiber. With this study, we show that the change in mechanical properties upon immersion in TRIS is dictated by the cladding surface reaction with the medium rather than the fiber geometry. This core-clad fiber exhibited good light transmission and the change in light transmission was assessed upon immersion in TRIS. The clad of the core-clad fiber was etched in phosphoric acid to reveal the core. Such process led to a decrease of the fiber mechanical properties. Upon immersion, for 10 days in TRIS, a drop of 50% of the initial light intensity was recorded ~~after 10 days in TRIS~~.

Owing to the ability to guide light effectively and to maintain decent tensile strength in vitro (~ 150-200 MPa after 6 wks in TRIS), this fiber looks promising for future use as a biosensing device in vivo.

Acknowledgement

The authors would like to acknowledge the financial support of the Academy of Finland through the Academy Research Fellow grant (275427), the Initial and follow-on funding for research costs (284492 and 312634) and Competitive Funding to Strengthen University Research Profiles (310359).

References

[1] L.L. Hench, R.J. Splinter, W.C. Allen, T.K. Greenlee, "Bonding Mechanisms at the Interface of Ceramic Prosthetic Materials," Journal of Biomedical Materials Research, Vol. 2, No. 1, (1971) 117-141

[2] S. Fagerlund, J. Massera, L. Hupa, M. Hupa, "T-T-T behaviour of Bioactive Glasses 1-98 and 13-93", Journal of European Ceramic Society, 32(11), (2012) 2731-2738

[3] J. Massera, S. Fagerlund, L. Hupa, M. Hupa, "Crystallization behavior of the commercial bioactive glasses 45S5 and S53P4", Journal of the American Ceramic Society, 95 (2012) 607-613

[4] B.C. Bunker, G.W. Arnold, J.A. Wilder, "Phosphate glass dissolution in aqueous solutions", Journal of Non-Crystalline Solids Volume 64, 3 (1984) 291-316

[5] A. Mishra, J. Rocherullé, J. Massera, "Ag-doped phosphate bioactive glasses: thermal, structural and in-vitro dissolution properties", Biomedical Glasses 2 (2016), 38–48

[6] J. Massera, Y. Shpotyuk, F. Sabatier, T. Jouan, C. Boussard-Plédel, C. Roiland, B. Bureau. L. Petit, N. Boetti, D. Milanese, L. Hupa, "Processing and characterization of novel borophosphate glasses and fibers for medical applications", Journal of Non-Crystalline Solids, 425 (2015) 52-60

[7] J. Massera, M. Vassallo-Breillot, B. Törngren, B. Glorieux, L. Hupa, "Effect of CeO_2 doping on thermal, optical, structural and in vitro properties of a phosphate based bioactive glass", Journal of Non-Crystalline Solids 402 (2014) 28–35

[8] E.A. Abou Neel, D.M. Pickup, S.P. Valappil, R.J. Newport, J.C. Knowles, "Bioactive Functional Materials: A Perspective on Phosphate-Based Glasses", Journal of Materials Chemistry, 19 (2009) 690-701

[9] R. Colquhoun, K.E. Tanner, "Mechanical behaviour of degradable phosphate glass fibres and composites-a review", Biomed. Matter., 11 (2015) 014105.

[10] J. Clement, J.M. Manero, J.A. Planell, "Analysis of the structural changes of a phosphate glass during its dissolution in simulated body fluid", Journal of Materials Science: Materials in Medicine, 10 (1999) 729–732.

[11] J.C. Knowles, "Phosphate based glasses for biomedical applications", Journal of Materials Chemistry, 13 (2003) 2395–2401.

[12] M.A. De Diego, N.J. Coleman, L.L. Hench, "Tensile properties of bioactive fibers for tissue engineering applications", Journal of Biomedical Materials Research Part A, 53 (2000) 199–203.

[13] J. Choueka, J.L. Charvert, H. Alexander, Y.H. Oh, G. Joseph, N.C. Blumenthal, W.C.

LaCourse, "Effect of Annealing Temperature on the Degradation of Reinforcing Fibers for Absorbable Implants, Journal of Biomedical Materials Research, 29 (1995) 1309–1315.

[14] I. Ahmed, M. Lewis, I. Olsen, J.C. Knowles, "Phosphate glasses for tissue engineering: Part 1. Processing and characterisation of a ternary-based P_2O_5-CaO-Na_2O glass system" Biomaterials, 25 (2004) 491–499.

[15] B. Gholamzadeh, H. Nobovati, "Fiber Optic Sensors, World of Academy of Science, Engineering Technology, 18 (2008) 297–307.

[16] J. Massera, I. Ahmed, L. Petit, V. Aallos, L. Hupa, "Phosphate-based glass fiber vs. bulk glass: Change in fiber optical response to probe in vitro glass reactivity", Material Science and Engineering C 37 (2014) 251–257.

[17] V. P. Gapontsev, S. M. Matitsin, A. A. Isineev, and V. B. Kravchenko, "Erbium glass lasers and their applications," Opt. Laser Technol. 14(4), 189–196 (1982).

[18] S. Jiang, M. J. Myers, and N. Peyghambarian, "Er^{3+} doped phosphate glasses and lasers," J. Non-Cryst. Solids 239 (1998) 143–148.

[19] D. Pugliese, N. G. Boetti, J. Lousteau, E. Ceci-Ginistrelli, E. Bertone, F. Geobaldo, and D. Milanese, "Concentration quenching in an Er-doped phosphate glass for compact optical lasers and amplifiers," J. Alloys Compd. 657 (2016) 678–683

[20] J. Massera, A. Kokkari, T. Narhi, L. Hupa, "The influence of SrO and CaO in silicate and phosphate bioactive glasses on human gingival fibroblasts", Journal of Materials Science: Materials in Medicine, 26 (2015) 196

[21] J. Massera, A. Haldeman, D. Milanese, H. Gebavi, M. Ferraris, P. Foy, W. Hawkins, J. Ballato, R. Stolen, L. Petit, K. Richardson, "Processing and characterization of core–clad tellurite glass preforms and fibers fabricated by rotational casting", Opt. Mater., 32 (2010) 582-588.

[22] M. Curie, A Lepape. Conductibilité thermique des gaz rares. J. Phys. Radium, 2 (1931) 392–397.

[23] E. Pirhonen, L. Moimas, M. Brink, "Mechanical properties of bioactive glass 9-93 fibres", Acta Biomaterialia, 2 (2006) 103-107

[24] E. Pirhonen, H. Niiranen, T. Niemelä, M. Brink, P. Törmälä, "Manufacturing, mechanical characterization, and in vitro performance of bioactive glass 13–93 fibers", Journal of Biomedical Materials Research: Part B, 77B (2006) 227-233

[25] N. Syam Prasad, J. Wang, R.K. Pattnaik, H. Jain, J. Toulouse, "Preform fabrication and drawing of KNbO3 modified tellurite glass fibers, Journal of Non-Crystalline Solids 352 (2006) 519–523.

[26] J.H. Campbell, T.I Suratwala, "Nd-doped phosphate glasses for high-energy/high-peak-power lasers", Journal of Non-Crystalline Solids, Journal of Non-Crystalline Solids, 263-264 (2000) 318-341.

[27] G.W. Sherer, A.R. Cooper, Thermal Stresses in clad-glass fibers, J. Am. Ceram. Soc., 63 (1980) 346-347

[28] D.A. Krohn, A. R. Cooper, Strengthening of glass fibers: I, Cladding, J. Am. Ceram., Soc., 52 (1969) 661-664)

[29] U.C. Paek, C.R. Kurkijan, Calculation of Cooling Rate and Induced Stresses in Drawing of Optical Fibers, J. Am. Ceram. Soc., 58 (1975) 330-335

[30] I. Ahmed, S.S. Shaharuddin, N. Sharmin, D. Furniss, C. Rudd, Core/Clad Phosphate Glass Fibres Containing Iron and/or Titanium, Biomedical Glasses, 1 (2015) 20-30.

[31] N. Sharmin, C.D.Rudd, A.J. Parsons, I. Ahmed, Structure, viscosity and fibre drawing properties of phosphate-based glasses: effect of boron and iron oxide addition, Journal of Materials Science, 51 (2016) 7523-7535.

[32] P.K. Gupta, Fractography of Fiberglass in: Bradt R.C., Tressler R.E. (eds) Fractography of Glass. Springer, Boston MA, (1994) 185-206.

[33] S. Cozien-Cazuc, A. Parsons, G. Walker, I. Jones, C. Rudd, "Effects of aqueous aging on the mechanical properties of P40Na20Ca16Mg24 phosphate glass fibres", Journal of Material Science, 43 (14) (2008) 4834–4839.

[34] R Colquhoun and K E Tanner, "Mechanical behaviour of degradable phosphate glass fibres and composites—a review", Biomed. Mater. 11 (2016) 014105.

[35] P. Haque, I. Ahmed, A. Parsons, R. Felfel, G. Walker, C. Rudd, "Degradation properties and microstructural analysis of $40P_2O_5$–$24MgO$–$16CaO$–$16Na_2O$–$4Fe_2O_3$ phosphate glass fibres", Journal of Non-Crystalline Solids 375 (2013) 99–109

[36] S. Inaba, S. Fujino, K. Morinaga, "Young's Modulus and Compositional Parameters of Oxide Glasses", Journal of The American Ceramic Society, 82 (1999) 3501-3507.

[37] L.G. Baikova, V.P. Pukh, Y.K. Fedorov, A.B. Sinani, L.V. Tikhonova, M.F. Kireenko, "Mechanical properties of phosphate glasses as a function of the total bonding energy per unit volume of glass", Glass Physics and Chemistry, 34 (2008) 126-131.

[38] J. Massera, A. Mishra, S. Guastella, S. Ferraris, E. Verné, "Surface functionalization of phosphate-based bioactive glasses with 3-aminopropyltriethoxysilane (APTS)", Biomedical Glasses, 2 (2016) 51-62.

[39] W. Weibull, "A statistical distribution of wide applicability", Journal of Applied Mechanics, 18 (1951), 293-297

[40] C.R. Kurkijan, M.J. Matthewson, J.M. Rooney, "Effects of Heat Treatment and HF Etching on the Strength of Silica Lightguides", Proceedings of SPIE - The International Society for Optical Engineering 5465, September 2004

[41] M. Bohner and J. Lemaitre, "Can bioactivity be tested in vitro with SBF solution?", Biomaterials, 30 (2009) 2175-2179

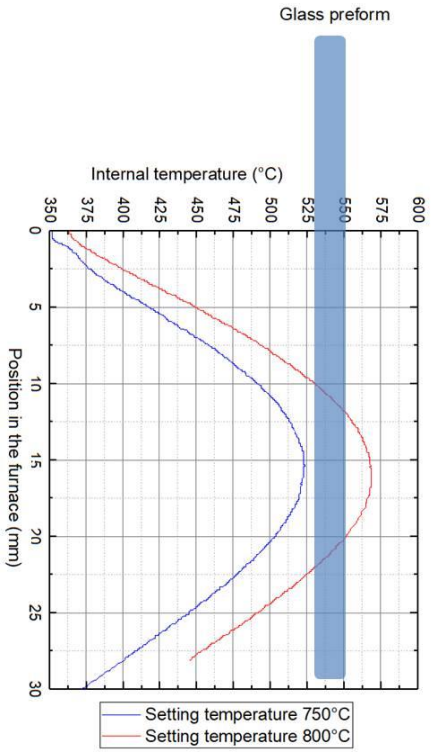

Figure 1: thermal profiles of the drawing tower furnace. The zero mm position correspond to the top of the heating element

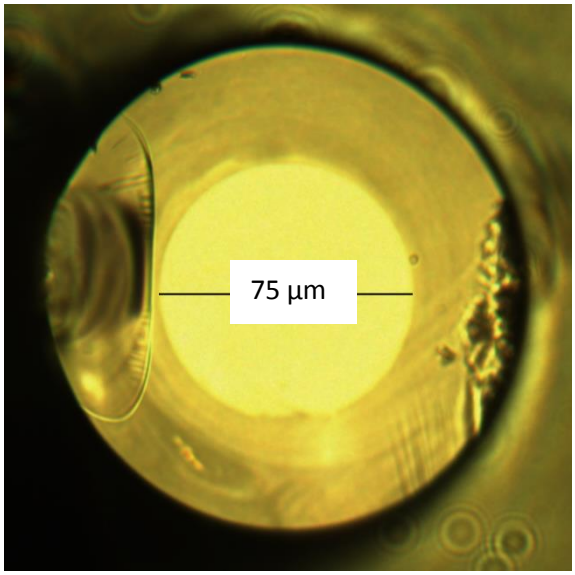

Figure 2 – Optical microscope image of the core-clad fiber cross section

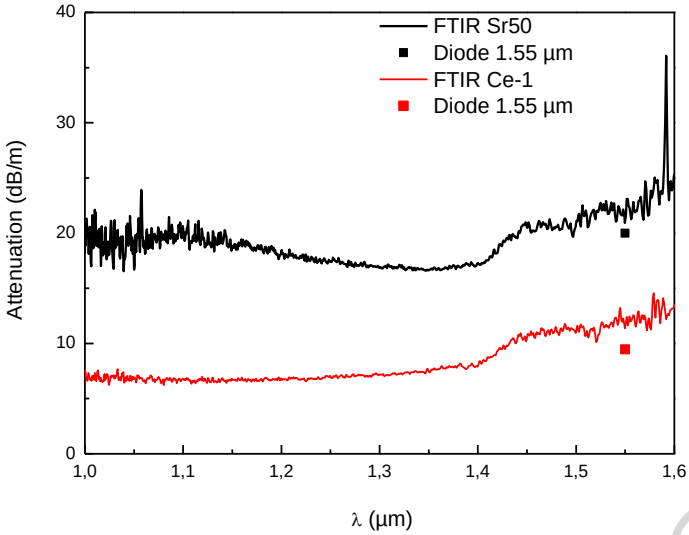

Figure 3– Attenuation of the single core fibers, Sr50 and Ce-1

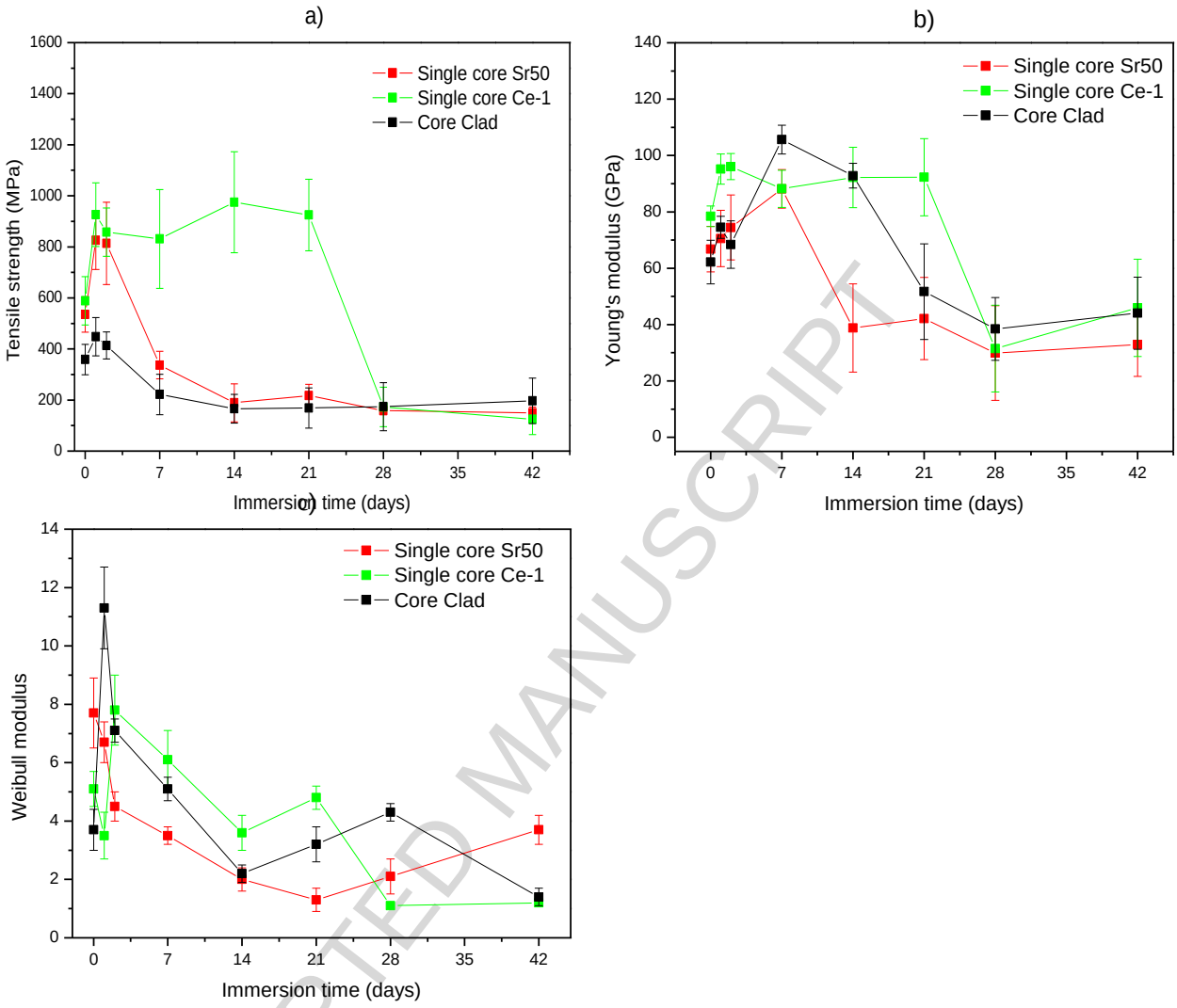

Figure 4 –a) Tensile strength, b) Young's modulus and c) Weibull modulus of single core and core-clad fibers immersed for up to 42 days in TRIS buffer solution

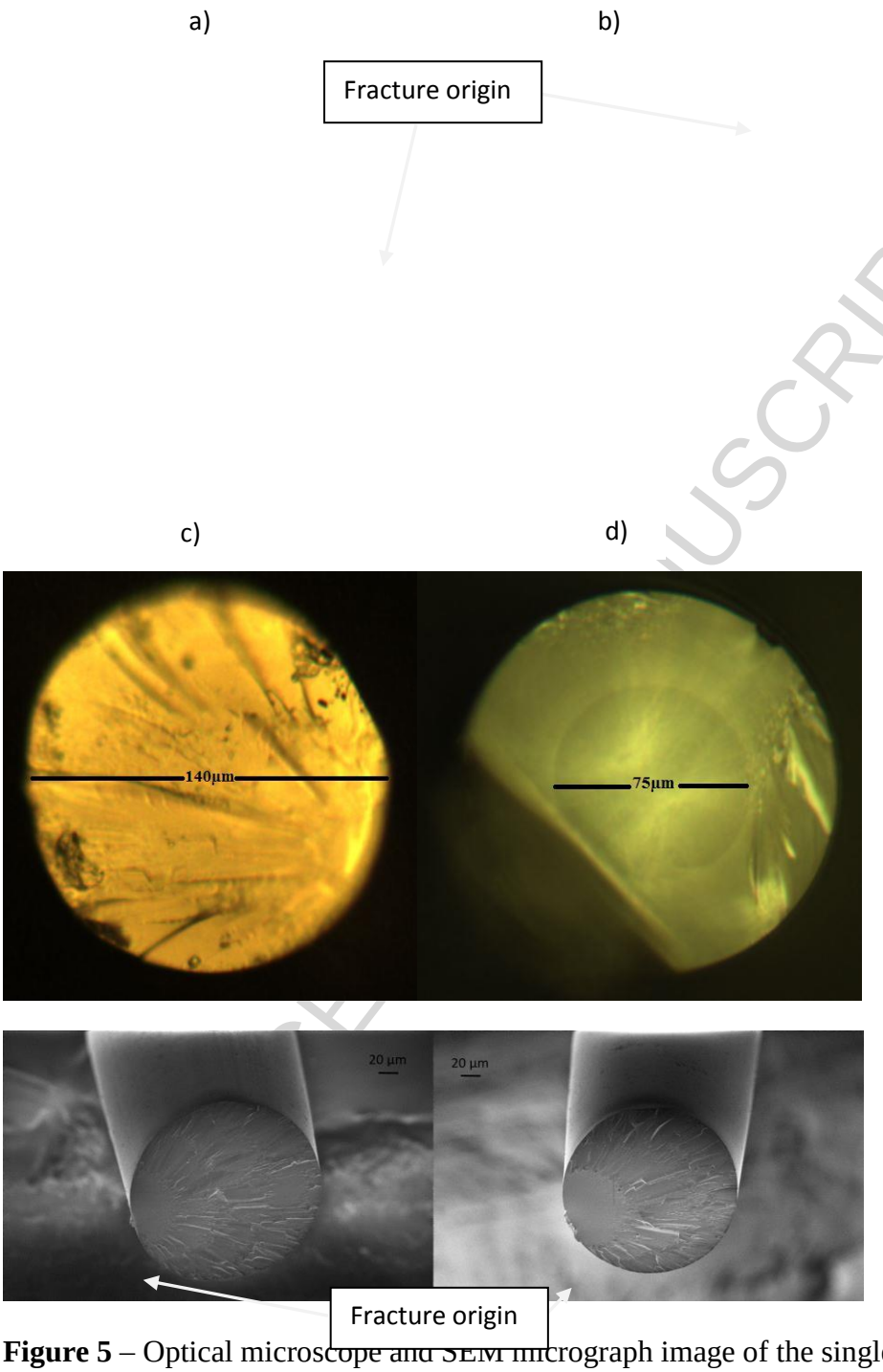

Figure 5 – Optical microscope and SEM micrograph image of the single core (Ce-1) a), c) and core-clad fiber b), d) cross section post tensile-test .

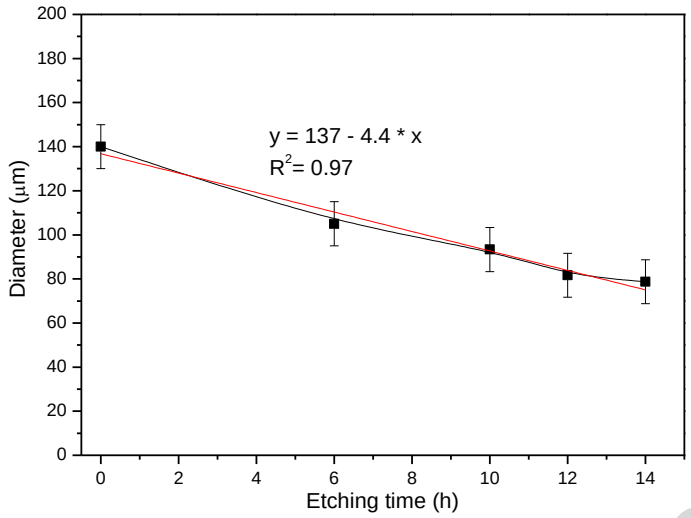

Figure 6 – Change in diameter of the core-clad fiber as a function of immersion time in 1M H_3PO_4

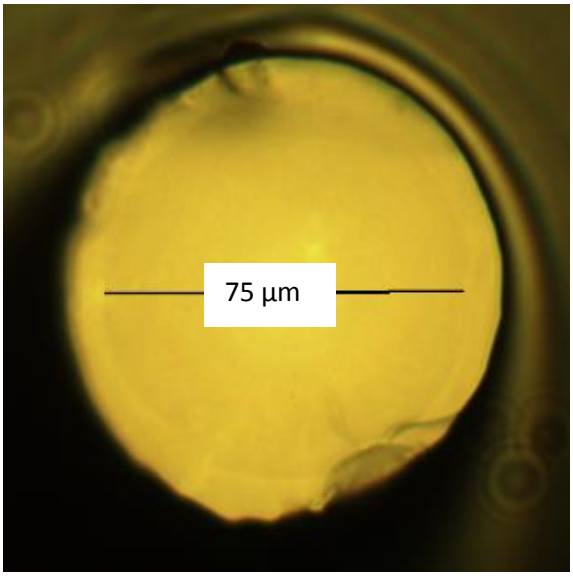

Figure 7 – Cross section of the core-clad fiber after 13h of etching.

a)

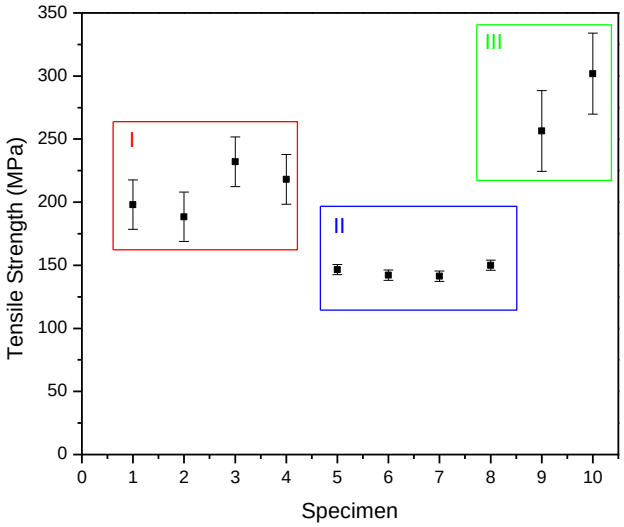

b)

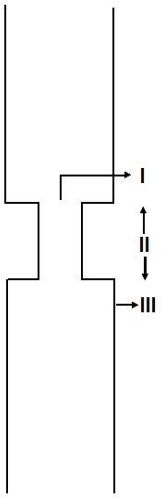

Figure 8 - a) Tensile strength of etched fibers on the basis of the region where fracture occurs, b) the different regions of fracture in the etched fiber

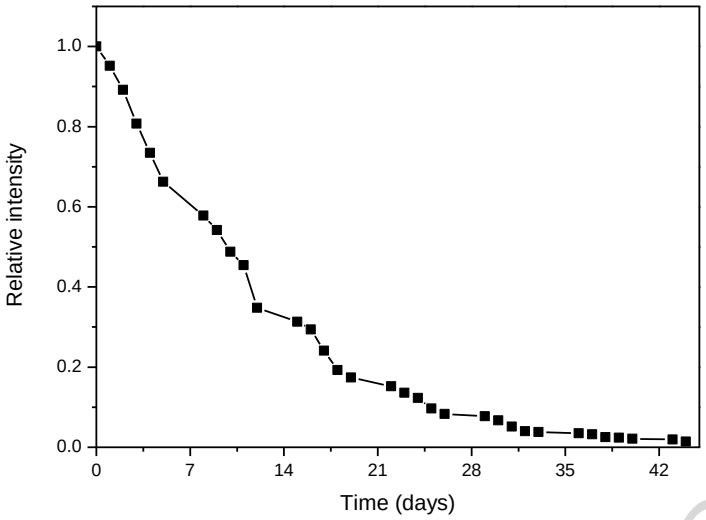

Figure 9 – Relative intensity of the output light at 680nm through the core-clad fiber as a function of immersion time in TRIS

a)

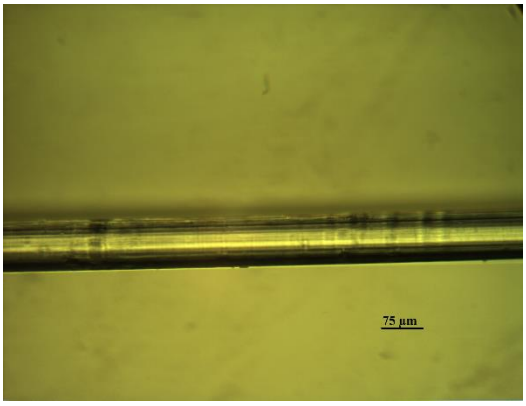

b)

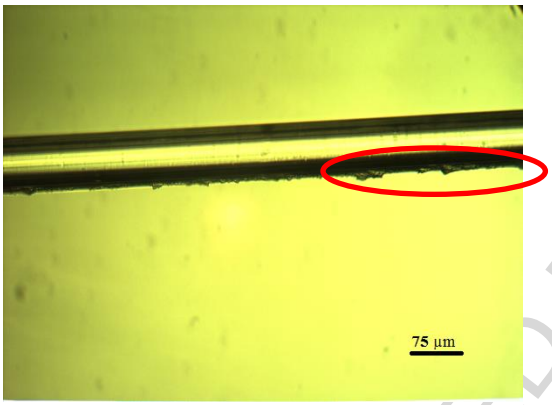

c) d)

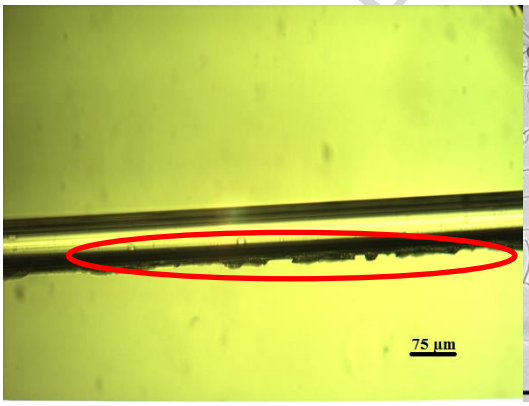

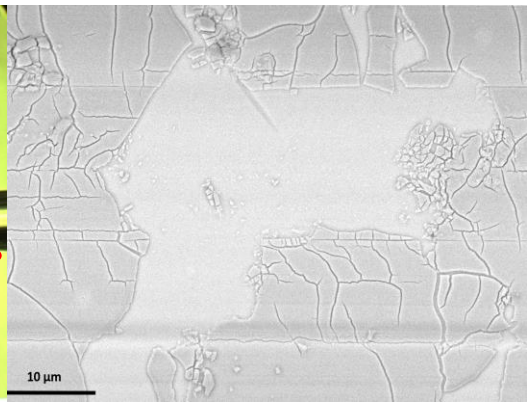

Figure 10 - Microscope images of the etched part of the core-clad fibers immersed for a) 7 days, b) 21 days and c) 42 days in TRIS and SEM image of the fiber surface at 42 days of immersion d). At 21 days surface layer starts to form (red circle). At 42 days thicker and more homogeneous reactive layer.

Highlights:

1. Impact of the fiber geometry (core vs core-clad fibers) on the mechanical properties (Tensile strength, Young's modulus and Weibull modulus).
2. Development of a protocol to etch away the cladding (of core-clad fibers) to generate a sensing region.
3. Impact of glass immersion in TRIS buffer solution on the optical properties of the etched core-clad fiber.
4. Impact of etching on the mechanical properties was also investigated.

This work will lay the base on using optical properties to probe protein and/or cell attachment at the surface of a fiber

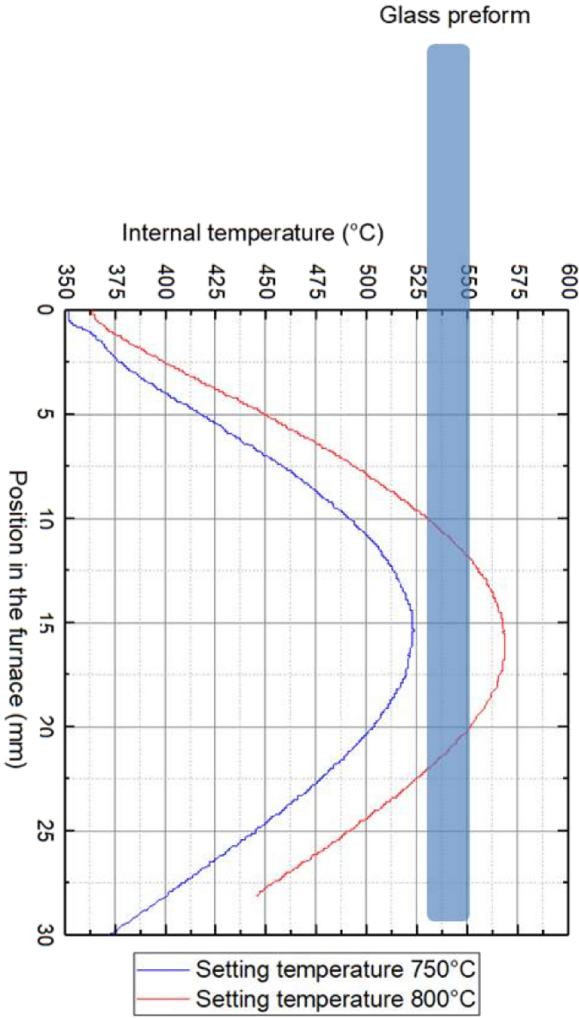
Glass preform
Internal temperature (°C)
350
375
400
425
450
475
500
525
550
575
600
Position in the furnace (mm)
0
5
10
15
20
25
30
Setting temperature 750°C
Setting temperature 800°C

Figure 1

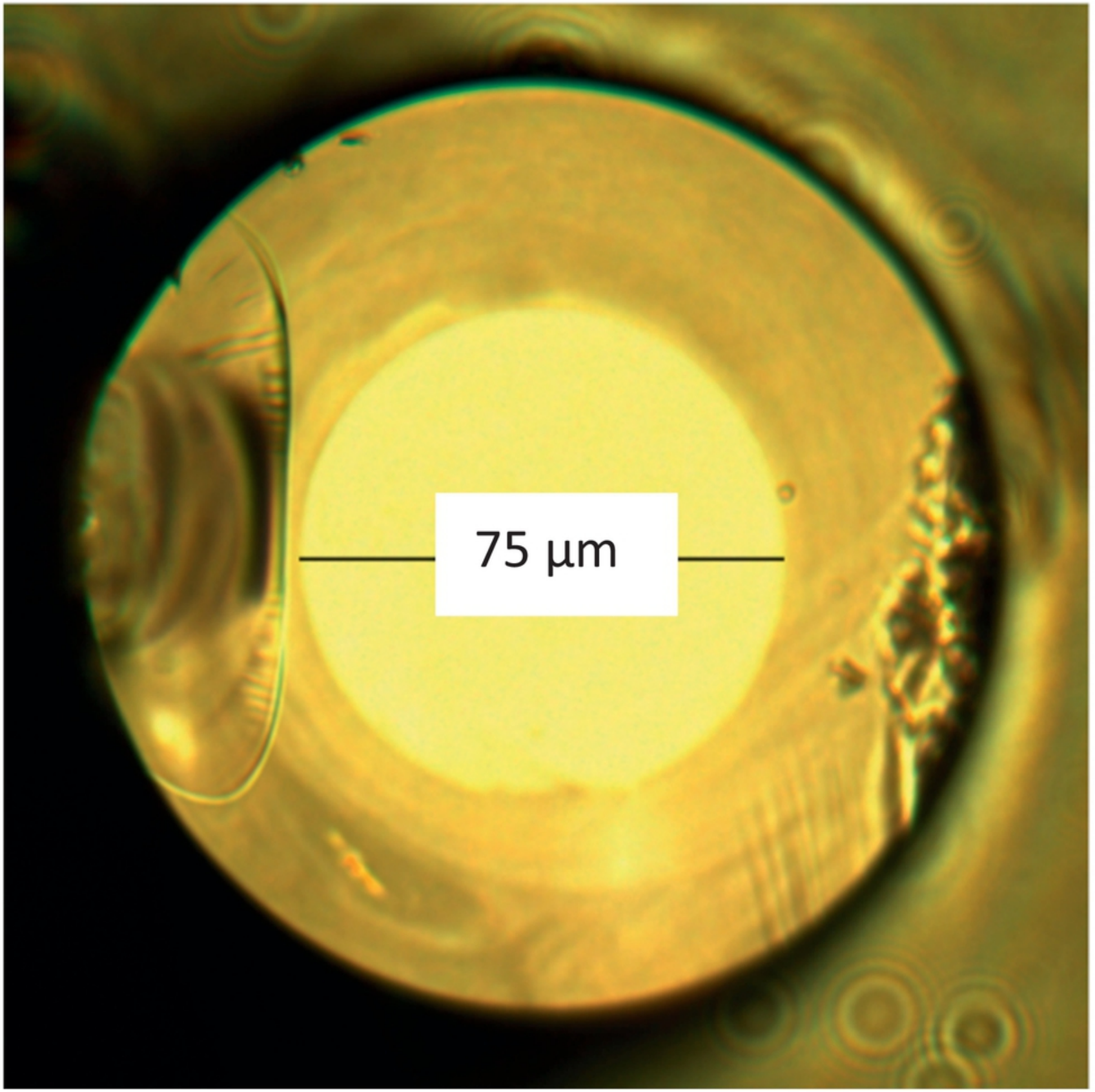

Figure 2

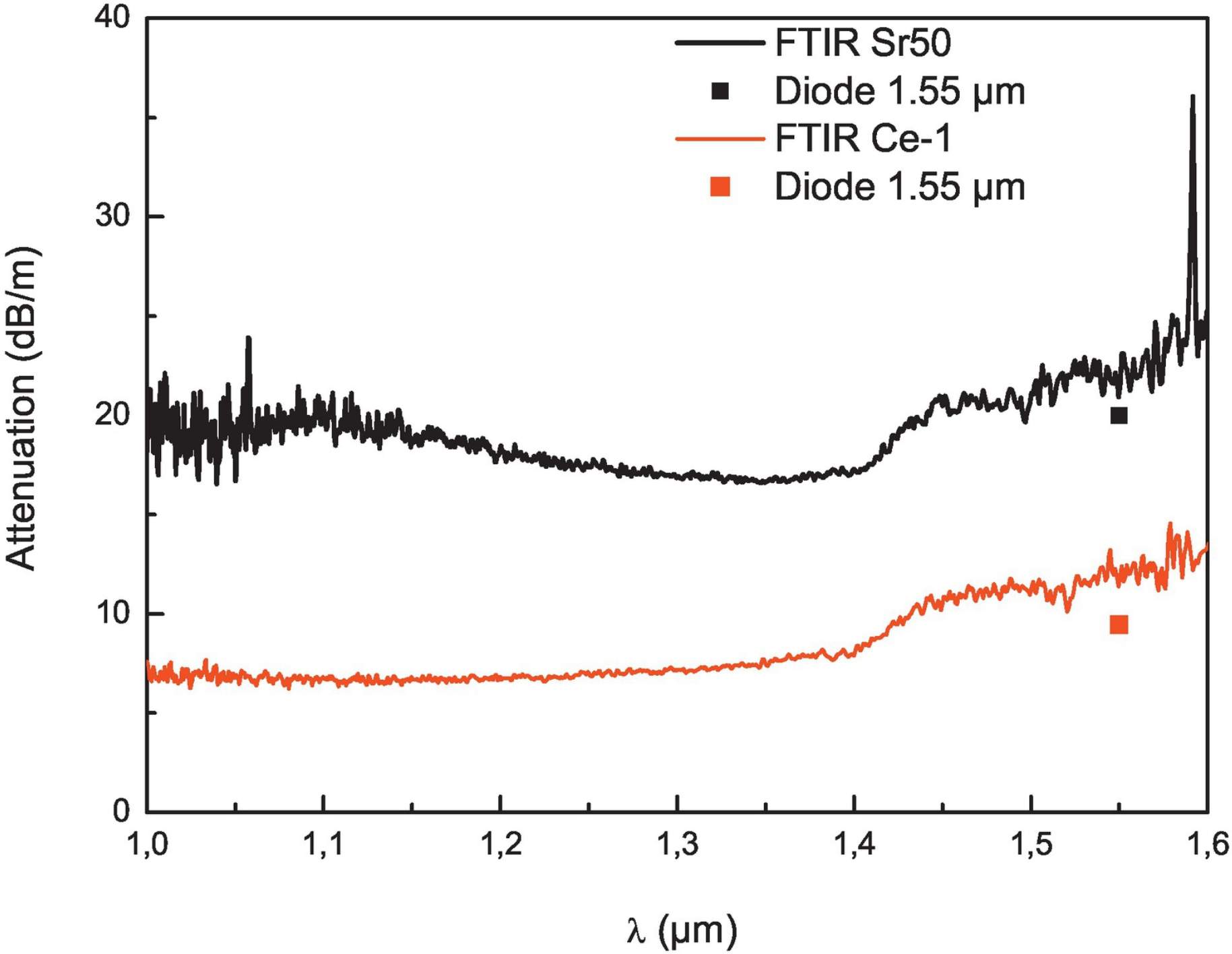
FTIR Sr50
Diode 1.55 µm
FTIR Ce-1
Diode 1.55 µm
Attenuation (dB/m)
40
30
20
10
0
1,0
1,1
1,2
1,3
1,4
1,5
1,6
λ (µm)

Figure 3

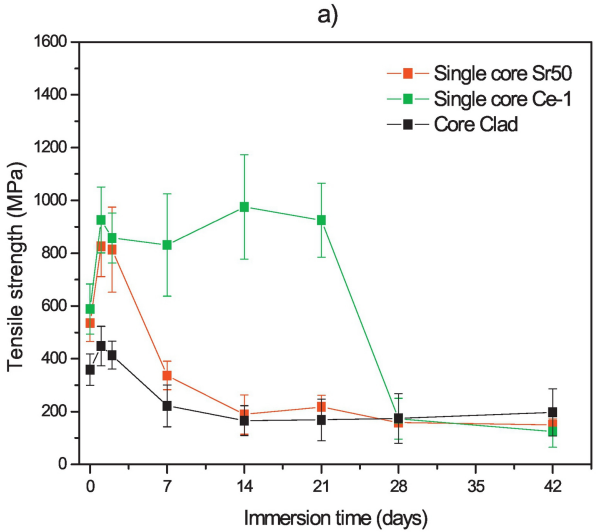
a)
Single core Sr50
Single core Ce-1
Core Clad
Tensile strength (MPa)
Immersion time (days)
0
200
400
600
800
1000
1200
1400
1600
0
7
14
21
28
35
42

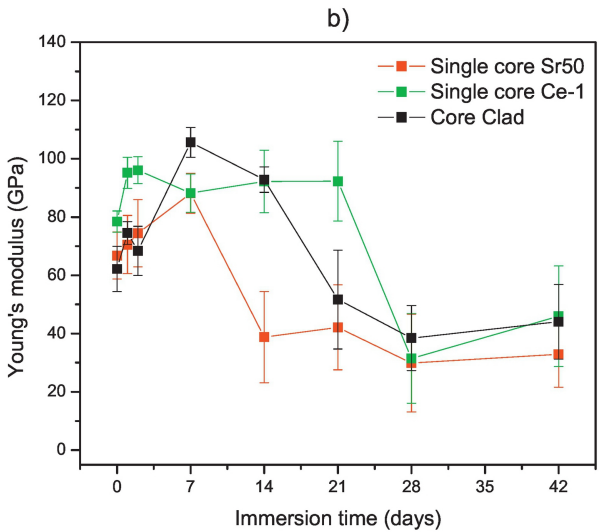
b)
Single core Sr50
Single core Ce-1
Core Clad
Young's modulus (GPa)
Immersion time (days)
0
20
40
60
80
100
120
140
0
7
14
21
28
35
42

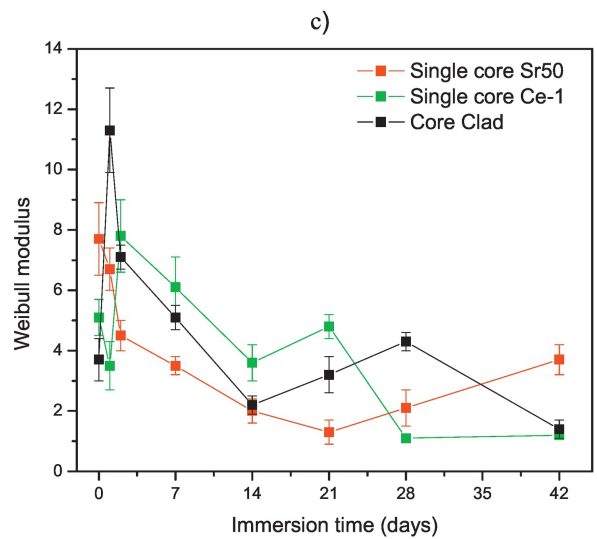
c)
Single core Sr50
Single core Ce-1
Core Clad
Weibull modulus
Immersion time (days)
0
2
4
6
8
10
12
14
0
7
14
21
28
35
42

Figure 4

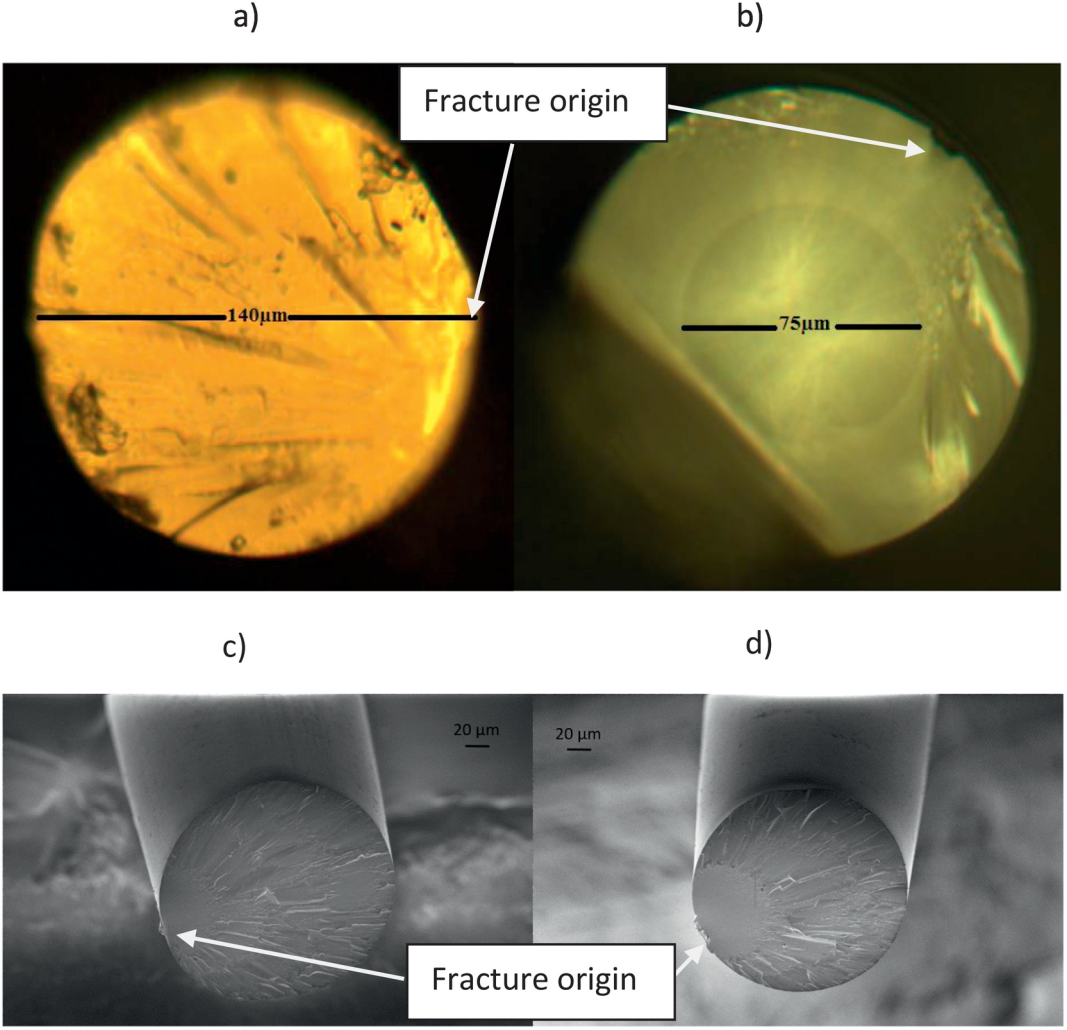

Figure 5

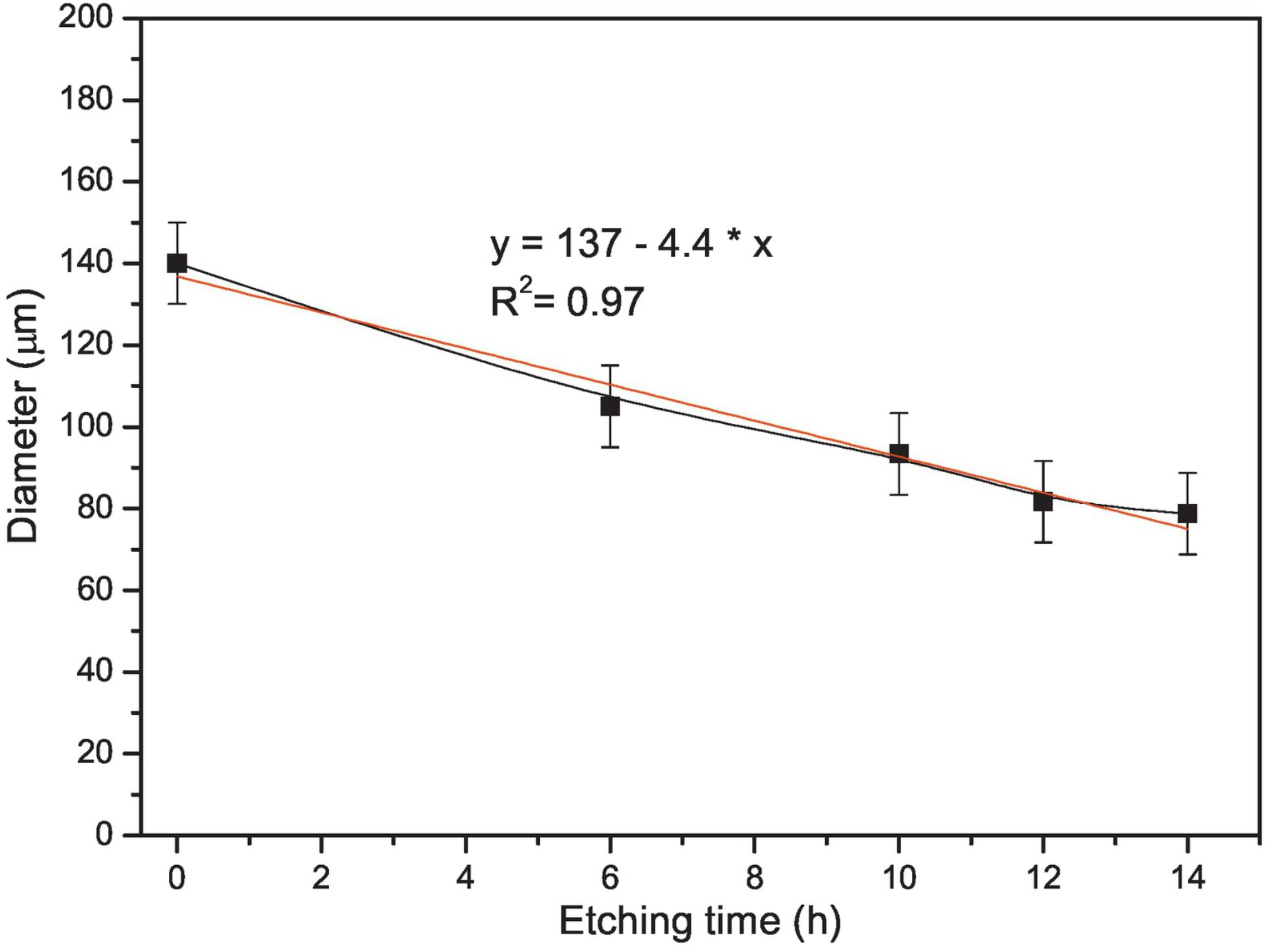
y = 137 - 4.4 * x
R2= 0.97
Diameter (µm)
Etching time (h)
0
20
40
60
80
100
120
140
160
180
200
0
2
4
6
8
10
12
14

Figure 6

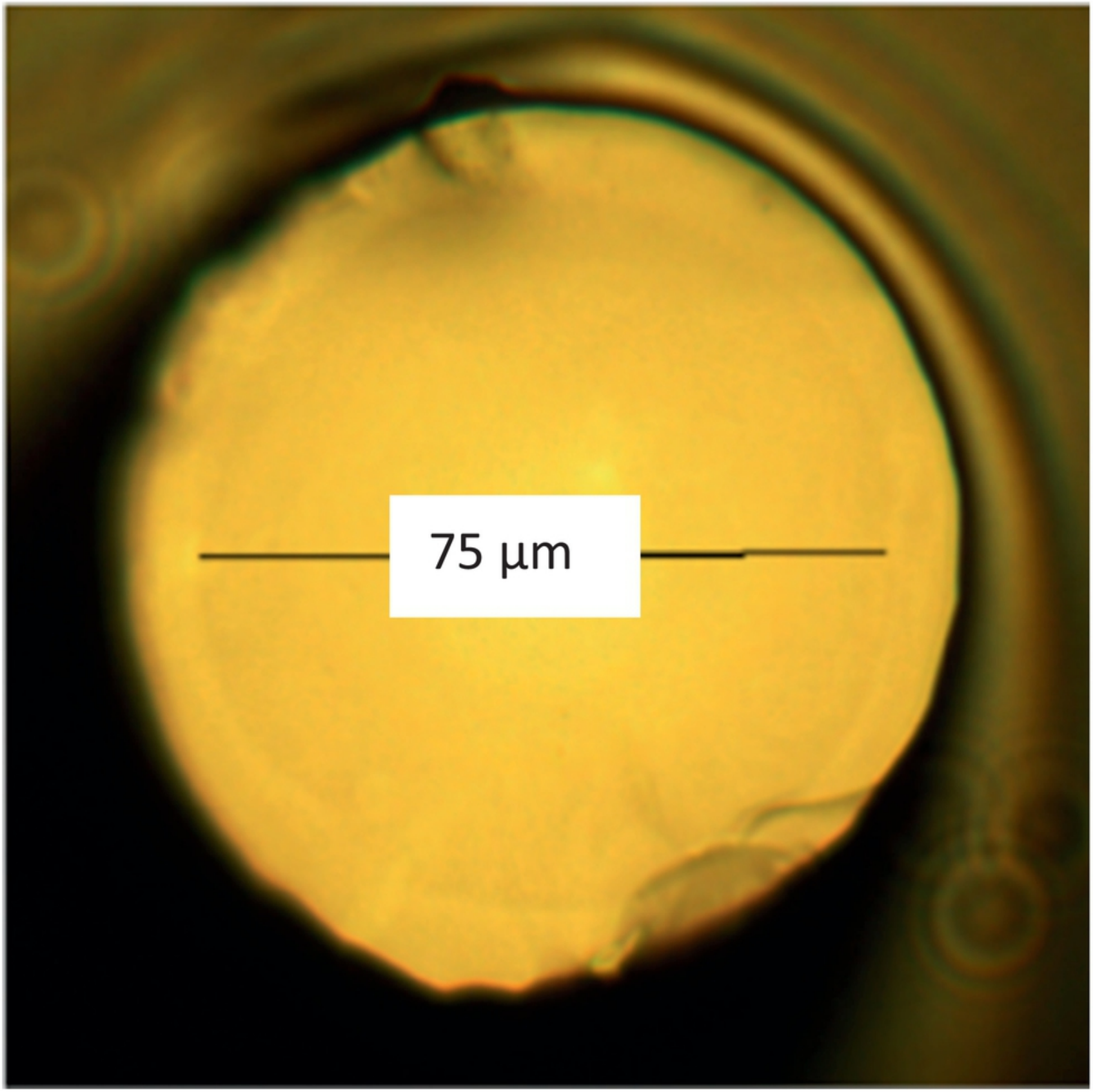

Figure 7

a)

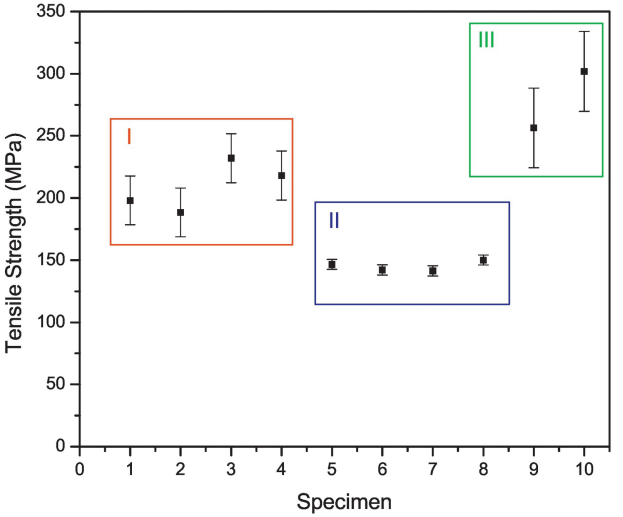
Tensile Strength (MPa)
Specimen
I
II
III
0
50
100
150
200
250
300
350
0
1
2
3
4
5
6
7
8
9
10

b)

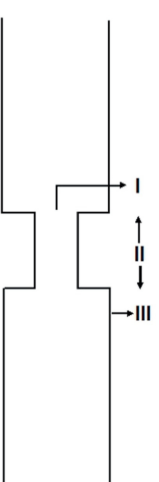
I
II
III

Figure 8

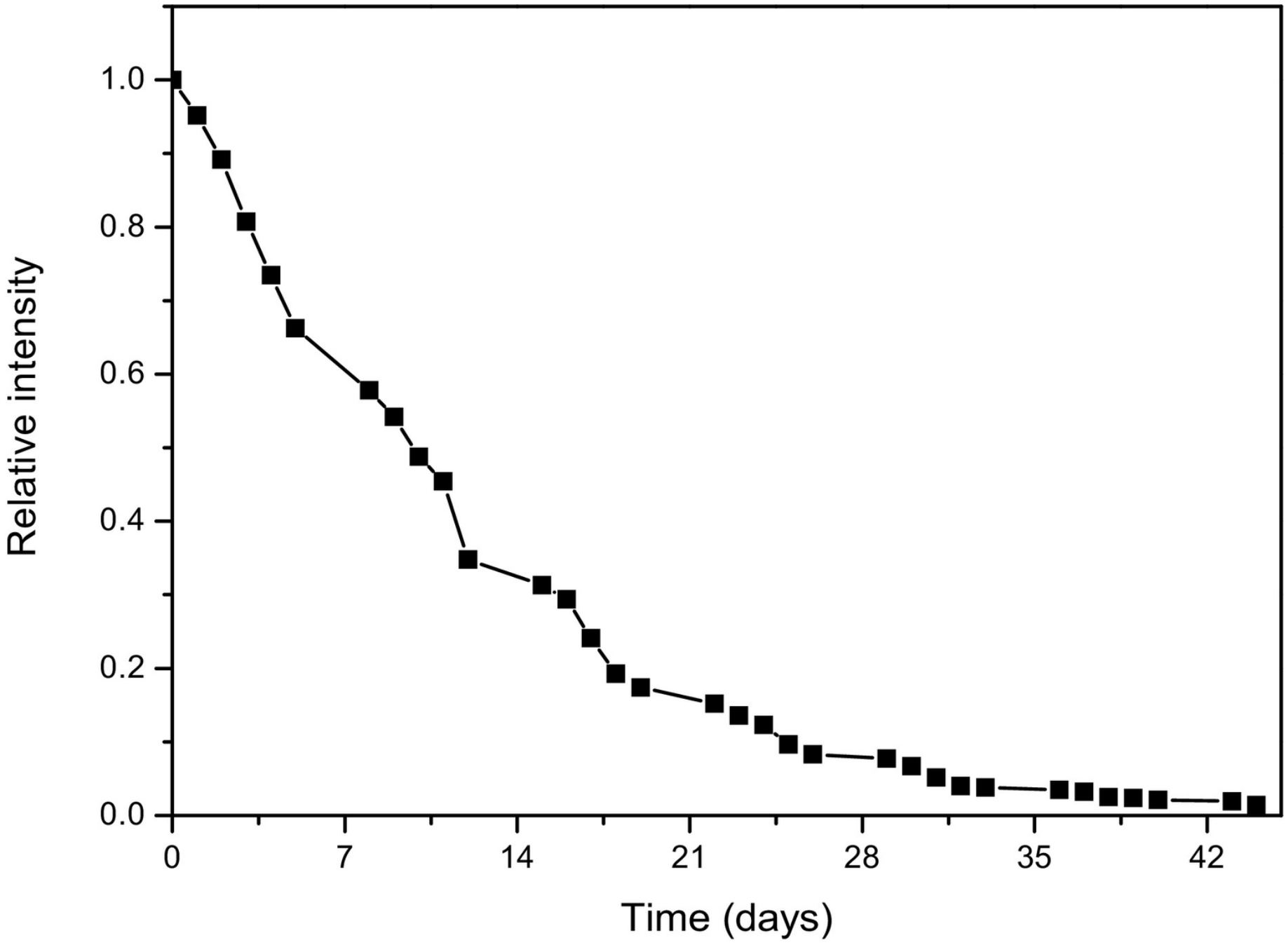

Figure 9

a)

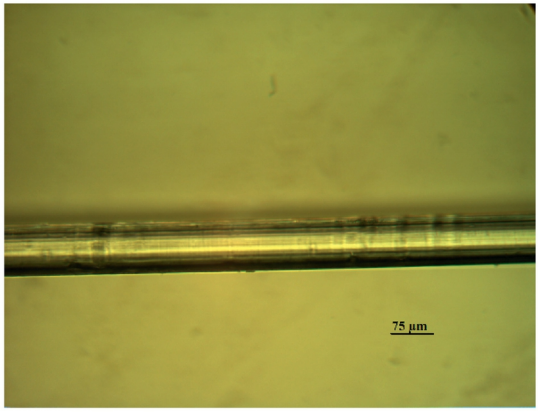

b)

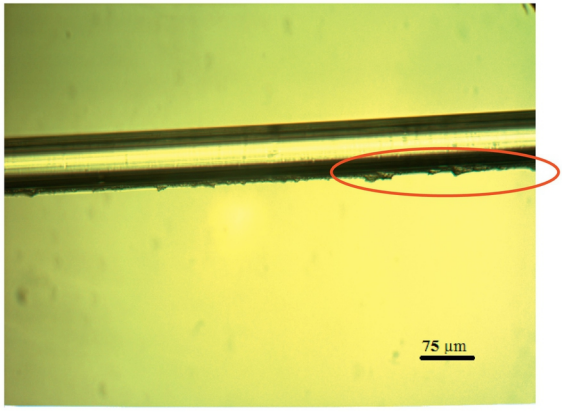

c)

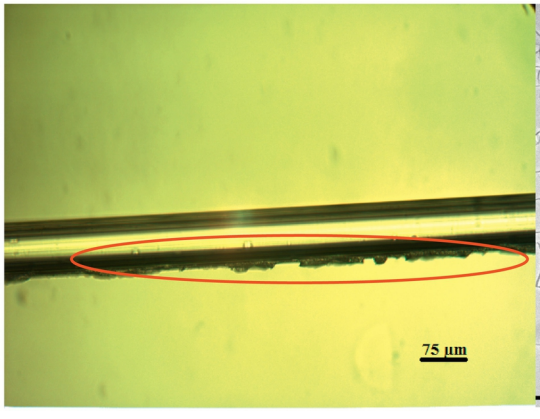

d)

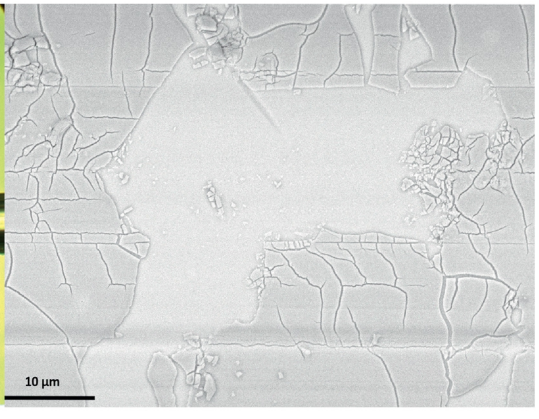

Figure 10